A fast algorithm for three-dimensional interpretations of single-well electromagnetic data*

Hung-Wen Tseng[1], and Ki Ha Lee[2]

Earth Sciences Division
Lawrence Berkeley National Laboratory
1 Cyclotron Road
Berkeley, CA 94720
1. e-mail: hwtseng@lbl.gov
2. e-mail: khlee@lbl.gov

ABSTRACT

An efficient inversion algorithm has been developed for three-dimensional (3D) interpretations for single-hole electromagnetic (EM) logging data based on a modified extended Born approximation (MEBA) scheme. The single-hole data was collected at an oil field undergoing CO_2 injection in southern California using a tool, Geo-BILT, developed by Electromagnetic Instruments, Inc (EMI). The tool is equipped with a multi-component source, and an array of multi-component receivers at different separations. The inversion result provides a reasonable electrical conductivity image to a distance of 10 m from the well, and illustrates several zones with lateral conductivity variations that could not be resolved with traditional induction logging tools. The computer cost of the inversion processes can be further reduced using a trivial multi-grid methodology.

INTRODUCTION

Electrical conductivity is related to the porosity, pore fluid conductivity, saturation, temperature, and clay content of rocks. This intrinsic relationship justifies the use of EM geophysical methods with applications to geohydrology, enhanced oil recovery monitoring, engineering geophysics, monitoring of environmental remediation processes, and geothermal exploration. Traditionally, EM induction logging is widely used for directly measuring the formation conductivity surrounding uncased wells. Such logging tools primarily consist of a

* Part of the results was presented at the 29th Workshop on Geothermal Reservoir Engineering: Stanford University, California, USA, 26-28 January, 2004.

magnetic dipole transmitter and a receiver in a coaxial configuration in line with the borehole axis. Due to this cylindrically symmetric nature of the source and receiver configuration, induction-logging data offers no information about the 3-D conductivity distribution in the vicinity of the borehole. The 3-D conductivity structure surrounding a borehole can only be characterized if multiple components of the magnetic fields due to various source polarizations are acquired (Alumbaugh and Wilt, 2001). Electromagnetic Instrument Inc. (EMI) has developed a single-hole induction logging system dubbed the Geo-BILT system. The tool consists of a three-component magnetic source and two three-component inductive receivers spaced at 2 and 5 meters, respectively, from the transmitter. This results in two 3x3 tensor data at two separations for a specific source depth. However, 3-D interpretations using such single-hole EM data is difficult because of the richness and complexity of the data and the very large number of discretized conductivity elements needed to represent a realistic earth model. Taking advantage of the computing efficiency of an algorithm based on a modified extended Born approximation (MEBA, Tseng et al., 2003), we developed an inversion code for interpreting EM data acquired in a single-hole environment. Following a brief description of the theory, synthetic data derived from simulating a thin sheet model is used to demonstrate the algorithm. Then data from an oil field in southern California is interpreted.

In discretized models, the number of cells used to represent a geological model plays a critical role in the computing efficiency and model resolution. The finer a conductivity model is divided into, the better the model resembles the realistic subsurface structure. However, this will increase the computing burden as a function of the cube of the number of cells and the non-uniqueness inherent in the inverse solutions. This means that a finely discretized model does not necessarily yield better inversion results. Vesnaver and Bohm (2002) illustrated that coarser cells usually result in robust images because finer models are dominated by the null space, and

pursuing for higher resolution images may often be worthless. Based on this perspective, we use a multi-grid scheme to further reduce the time required for 3D EM inversions.

THE MEBA FOR 3-D SIMULATION AND INVERSION

Based on the integral equation method (Hohmann, G. W., 1975) for geophysical EM simulations, the magnetic field, **H**, at a location, $\mathbf{r}_r$, produced by an EM source can be evaluated using

$$\mathbf{H}(\mathbf{r}_r) = \mathbf{H}_b(\mathbf{r}_r) - iw\mu_0 \int_{V_s} \overline{\overline{\mathbf{G}}}^{H}(\mathbf{r}_r,\mathbf{r}')\Delta s(\mathbf{r}')\cdot\mathbf{E}(\mathbf{r}')d\mathbf{r}', \quad (1)$$

where $\mathbf{H}_b$ is the primary magnetic field due to the source; Δs is the conductivity anomaly in a layered subsurface; $\mathbf{E}(\mathbf{r}')$ is the total electric field in the anomaly; $\overline{\overline{\mathbf{G}}}^{H}$ is the Green's function relating the magnetic field at $\mathbf{r}_r$ to a current source at $\mathbf{r}'$; w is the angular frequency, μ_0 is the free space magnetic permeability, and i is $\sqrt{-1}$. The electric field, $\mathbf{E}(\mathbf{r}')$, may be derived by solving an integral equation for a discretized model. However, the technique becomes impractical as the number of the discretized model parameter is increased. This computational hurdle can be avoided using approximate techniques, such as the modified extended Born approximation (Tseng et al., 2003). With this approach, the electric field in the conductivity anomaly can be approximated using

$$\mathbf{E}(\mathbf{r}') \approx \overline{\overline{\mathbf{G}}}^{m}(\mathbf{r}')\cdot\mathbf{E}_b(\mathbf{r}') \quad (2)$$

where $\overline{\overline{\mathbf{G}}}^{m}$ is a 3x3 tensor expressed as:

$$\overline{\overline{\mathbf{G}}}^{m}(\mathbf{r}') = \left[\overline{\overline{\mathbf{I}}} + i\omega\mu_0\sigma(\mathbf{r}')\int_{V_s} \overline{\overline{\mathbf{G}}}^{E}(\mathbf{r}',\mathbf{r}'')\frac{\Delta\sigma(\mathbf{r}'')}{\sigma(\mathbf{r}'')}d\mathbf{r}''\right]^{-1} \quad (3)$$

Here, σ is the total conductivity; $\overline{\overline{\mathbf{G}}}^{E}$ is the Green's tensor relating the electric field at $\mathbf{r}'$ to a current source at $\mathbf{r}''$, and $\overline{\overline{\mathbf{I}}}$ is a unit tensor. The integral in (3) is a convolution between $\overline{\overline{\mathbf{G}}}^{E}$ and the anomalous media conductivity. Therefore, application of the fast Fourier transform

technique to the integral makes the MEBA code efficient for low frequency EM 3-D simulation. Computer cost using the MEBA algorithm primarily increases as the square of the number of cells in the vertical direction, in contrast to the cube of the total number of cells for the integral equation method.

The MEBA code is incorporated into a 3-D non-linear inversion algorithm based on a least-squares approach following Oldenburg et al. (1993). An updated model, $\mathbf{m}^{k+1}$, is derived by solving the following system of equations:

$$\left[\bar{\bar{\mathbf{J}}}^T\bar{\bar{\mathbf{W}}}_d^T\bar{\bar{\mathbf{W}}}_d\bar{\bar{\mathbf{J}}}+\lambda\bar{\bar{\mathbf{W}}}_m^T\bar{\bar{\mathbf{W}}}_m\right]\mathbf{m}^{k+1}=\bar{\bar{\mathbf{J}}}^T\bar{\bar{\mathbf{W}}}_d^T\bar{\bar{\mathbf{W}}}_d\left[\bar{\bar{\mathbf{J}}}\mathbf{m}^k-\mathbf{d}(\mathbf{m}^k)+\mathbf{d}^{obs}\right]. \tag{4}$$

Here, the superscript *T* denotes transpose of the matrix; *k* is the iteration number and $\mathbf{d}(\mathbf{m}^k)$ is a column vector representing the calculated system response to the subsurface conductivity model, $\mathbf{m}^k$; $\bar{\bar{\mathbf{W}}}_d$ is a square weighting matrix that assigns a relative importance to each data point. Usually it's a diagonal matrix with the elements equal to the inverse of the noise in the observation. The matrix, $\bar{\bar{\mathbf{W}}}_m$, determines how the model is biased. In this study, a smoothness criterion based on spatial gradient is used to constrain the inversion procedure. The variable l in (4) is a Lagrange multiplier that controls the degree of smoothness of the model. The Jacobian matrix, $\bar{\bar{\mathbf{J}}}$, which is the change in the EM field for each source-receiver pair due to the perturbation of each element of the discretized conductivity model, can be approximated based on the MEBA technique and an adjoint Green's function approach (McGillivray, et al. 1994, and Spies and Habashy, 1995):

$$\mathbf{J}_{nj}\approx -i\omega\mu_0\left(\bar{\bar{\mathbf{\Gamma}}}_j^m\cdot\mathbf{E}_{\mathrm{b},j}^*\right)\cdot\left(\bar{\bar{\mathbf{\Gamma}}}_j^m\cdot\mathbf{E}_{\mathrm{b},j}\right)\Delta\mathrm{V}_j\,. \tag{5}$$

Here, n indicates the n-th data (magnetic field), ΔV_j is the volume of the j-th descretized cell, and $\mathbf{E}_{b,j}$ and $\mathbf{E}^*_{b,j}$ are the primary electric fields in the conductivity inhomogeneity due to the real transmitter and a fictitious source at the receiver location, respectively.

Being such a critical element for the non-linear inversions, an analysis of the Jacobian matrix is useful in understanding the sensitivity and resolving ability of a specific survey configuration. Alumbaugh and Wilt (2001) presented in detail the sensitivity functions for all of the nine possible transmitter-receiver polarizations for single-hole EM surveys. It was demonstrated that, for the co-axial transmitter-receiver configuration and in traditional induction logging, the cylindrically symmetric pattern of the sensitivity function about the borehole makes 3-D structures surrounding the borehole impossible to resolve. Other asymmetric measurements, such as a horizontal field due to a vertical source, must be collected to obtain the 3-D conductivity structure surrounding the borehole.

For the inversion, analysis of the sensitivity matrix also helps in determining another important factor, the data-weighting matrix in (4). Due to the proximity between the source and receivers, the secondary co-axial and the co-planar data are measured in the dominant presence of the primary field due to the source. For example, assuming a vertical borehole in a 0.2 S/m whole space, at 6 kHz, the sensitivity function for a vertical magnetic dipole source and a vertical magnetic field receiver pair with a 5 m separation displayed in Figure 1(a). Here, the real and imaginary parts of the function are expressed as the logarithm of their values normalized to the corresponding maximum of the Jacobian for this configuration, with a value of ± 3 assigned to the locations where the maximum values occur and all values less than 1/1000 of the maximal assigned to 0. Both the real and imaginary parts are about the same magnitude relative to their corresponding maximum. However, if the sensitivity is normalized to the primary magnetic field, as shown in Figure 1(b), the real component is almost negligible if system noise is taken into account. In other words, only the imaginary part of the magnetic field contains significant

and measurable signal that carries the information about the conductivity structure surrounding the borehole.

NUMERICAL SIMULATIONS

Originally designed for cross-hole and borehole-to-surface configurations for vertical sources and receivers only, the MEBA code has been modified for the single-hole case for any combination of the source and receiver polarizations. To verify the performance of the modified code, synthetic data from simulating a horizontal conductive plate model depicted in Figure 2 is used for inversion. Here, in a homogeneous 0.2 S/m media, the center of the square sheet, which has a dimension of 5x5x1 m and a conductivity of 1 S/m, is placed 5 m from a vertical borehole while its edges are parallel to the two horizontal coordinates, X and Y. The separation between the transmitting and the receiving units is kept at 5 m and the center of the array runs from 3.5 m above the level of the plate to 7.5 m below this level at 1 m intervals. An integral equation algorithm developed by Wannamaker et al. (1985) was used to compute the synthetic data at a frequency of 6 kHz.

Assuming only the vertical coaxial component, Hz, is available (Figure 3), which is the case for traditional induction logging, a cylindrically symmetric conductivity image surrounding the well at the depth of the simulated conductive plate can be obtained as illustrated in Figure 4. The location of the simulated plate is indicated by the dashed square. Though the conductivity anomaly is found at the right depth, its azimuthally distribution cannot be resolved. In addition, the value of the conductivity of the anomalous body cannot be properly recovered due to the smoothness criteria used to constrain the non-linear inversion. Adding the other two orthogonal horizontal magnetic fields, H_x and H_y as shown in Figure 3, to the inversion, the depth and horizontal location of the conductive body can be clearly recovered as presented in Figure 5.

However, the radial extension of the conductivity distribution derived from the inversion is still ambiguous.

As mentioned previously, to achieve reasonable inversion results careful consideration of the weighting on the data is critical. This is particularly important in case of the co-axial data, because the primary magnetic field is dominant over the secondary field. After testing various combination of weighting coefficients for the vertical magnetic field, we decided to use the weighting on the imaginary part of the field 1000 times that for the real part. For the horizontal magnetic components, both real and imaginary parts are equally weighted since direct coupling, i.e., the primary magnetic field, between the vertical source and the calculated horizontal field is absent.

THE GEO-BILT SYSTEM, FIELD DATA, AND INVERSION RESULTS

A set of single-hole data was collected by EMI with the Geo-BILT system at a Chevron oil field in southern California during a CO_2 pilot injection project. The area has been undergoing water flooding since 1995 for oil recovery purposes (Hoversten, et. al, 2003). Four boreholes originally used for water injection have been converted for CO_2 injection started in September 2000. Figure 6 displays the surface projection of one of the CO_2 injection boreholes, 11-8WR, and two fiberglass-cased wells, OB-C1 and OB-C2, used for monitoring the progress of the injection. OBC-2 was about 80 ft to the south of OBC1 and the injection well, 11-8WR, was about 20 ft, on the eastern side, off the plane including OB-C1 and OB-C2. Cross-hole EM data was collected before the commencement of the injection and a set of single-hole data was acquired in May 2001 in the well OB-C1. Only the single-hole data and its interpretation are presented here.

From data obtained with the Geo-BILT, only the data with a vertical source and 5 m separation at 6 kHz is used for interpretation, due to the fact that data at this separation offers

more volumetric coverage around the borehole. A total of 123 source depths varying from 427 m to 549 m depth at 1 m intervals were selected. The calibrated magnetic fields in all three coordinate directions are illustrated as the blue lines in Figure 7. Here, the center between the transmitter and the receivers is used for labeling the depth of the data. The inversion domain, between 422 to 559 m in depth, was a 21x21x137 m volume divided into21x21x137 cells. The initial model was a homogeneous half-space with a conductivity of 0.4 S/m, which gives the best data fit for the initial model. The inversion took about 26 hours for 11 iterations using a COMPAQ Alpha workstation. The induction logging data was not used to constrain the inversion because the logging data may offer false information of the 3D conductivity distribution in this case.

The simulation data for the final model is displayed as the red lines in Figure 7. Data mismatch for the vertical magnetic field is more obvious than the other two horizontal components. This may be due to the overwhelming dominance of the primary magnetic field over the secondary field for this component, and the real part of the field was almost neglected due to the data weightings. The conductivity distribution is presented in Figure 8 in two orthogonal vertical panels centered at OB-C1: one in the north-south direction containing the two observation boreholes (Figure 8(a)) and the other in the east-west direction (Figure 8(b)). The induction logging data in OB-C1 acquired in September 2000 is also displayed in Figure 8(d) for reference. The conductivity structure characteristics surrounding OB-C1 compares reasonably well with the logging data. However, the results show a major lateral conductivity variation around the borehole between the depths of 507 and 525 m, which is the primary producing layer at the site. The inhomogeneities are also manifested by the relatively significant anomalies in the two horizontal magnetic fields at the same depth. The horizontal slice of the conductivity distribution at the depth of 513 m, which is illustrated in Figure 8(c), displays a trend that the conductivity is smaller on the north-west side of OB-C1 than on the south-east side of the well.

This indicates that CO2 has been replacing the more conductive brine from the injection well, 11-8WR. Other minor lateral inhomogeneity can be observed at about 437 and 453 m, which are also apparent from the calibrated horizontal magnetic fields.

A multi-grid scheme for improving inversion efficiency

We have demonstrated the efficiency using the MEBA algorithm for efficient EM data inversion. Its performance can be further improved if the scheme can be adopted for parallel computing. However, similar improvement can be achieved by reducing the number of cells used to discretize the model, without sacrificing the resolution of the inversion. Vesnaver and Bohm (2002) demonstrated that the use of a large number of cells composing a velocity model for seismic tomography resulted in the non-uniqueness problem due to the null space involved in the inversion. Based on the perspective, an empirical multi-grid scheme is attempted to interpret the Lost Hills single-hole EM data described previously to test if computing cost and time used for 3-D inversions can be further reduced.

For this demonstration, the number of sources used for the single-hole data inversion is reduced to a half of the original data set, i.e., the number of source locations is 63 now and they are selected at 2 m intervals. As sketched in Figure 9, the background media is divided into 2x2x2 m cells and thus results in 11x11x70 unknowns, one eighth of the number used previously. The first transmitter is located at the center of the cell and inversion using the MEBA code is carried out. The conductivity images in two perpendicular vertical planes, the same as shown in Figures 8(a) and (b), centered at OBC1 are displayed in the columns labeled as 'Grid 1' in Figures 10(a) and (c), respectively. Now, the cells composing the model are moved down by 0.5 m relative to the first grid and the inversion is carried out again. The outcome is illustrated in the column labeled as 'Grid 2'. The same process is repeated two more times so that in the last grid ('Grid 4') the cell centers have been moved 1.5 m down from the EM source.

The derived conductivity images are displayed in the columns labeled as 'Grid 3' and 'Grid 4', respectively. The four inverted conductivities are projected to the same grid for 1 m^3 cells in the previous section and averages are taken to derive the final conductivity for each cell. The resultant contour plot is show in Figures 10(b) and (d), respectively, for the two perpendicular vertical planes. A comparison between Figures 8(a), (b), 10(b), and (d), clearly shows the two results matched remarkably well in patterns. The conductivity, however, derived using the coarser grids is about 0.1 S/m higher than that using the finer grids. Computer time for each of the multi-grid inversion takes only one sixth of that required for the model composed of $1m^3$ cells. The improvement in the efficiency is due to the fact that the number of cells discretizing the domain in the vertical direction is reduced to half of the 1 m^3 domain, as well as the number of source locations.

The cells composing the domain for inversion are moved only in the vertical direction in this demonstration. Lateral shift of the discretization is not considered as it does not maintain the symmetric pattern of the grid with respect to the borehole. Because the inversion for the four grids are independent from each other, the computation can be conducted using four workstations, or a multi-node station in a 'parallel computing' style without modifying the original algorithm for such purpose. In addition, demand for computer memory is also reduced dramatically because of less unknowns for the inversion. However, finding the optimal data density, grid size, and number of grids for this approach still needs to be explored.

SUMMARIES

We have illustrated that conductivity distribution and variation around a borehole can be obtained using EM single-hole data with the efficient 3-D inversion algorithm, MEBA. Multi-component magnetic fields and appropriate data weightings are required to complete the task. The 3-D inversion results on the Lost Hills clearly indicate the progress of the front of CO_2

injection. However, the definition of the radial extension of the inverted conductivity structure from the borehole remains ambiguous. Further studies will be necessary to alleviate this uncertainty by considering alternative model constraints, multi-frequency data, and additional transmitter-receiver offsets. An inversion scheme based on various grids of the model reduces the computing cost while inverted image quality using smaller models (coarser grids) is not necessarily sacrificed. However, finding an optimal grid size should improve the performance of the algorithm and this should not be overlooked in the future.

ACKNOWLEDGEMENTS

This work was supported by the Assistant Secretary for Energy Efficiency and Renewable Energy, Office of Wind and Geothermal Technologies, and Office of Basic Energy Science of the U.S. Department of Energy under Contract No. DE-AC03-76SF00098. We are also grateful for the partial financial support and field data offered by Electromagnetic Instrument, Inc.

REFERENCES

Alumbaugh, D. L., and Wilt, M. J., 2001, A numerical sensitivity study of three dimensional imaging from a single borehole: Petrophysics, 42, 19-31.

Hohmann, G. W., 1975, Three-dimensional induced polarization and electromagnetic modeling: Geophysics, 40, 309-324.

Hoversten, G. M., Gritto, R., Washbourn, J, and Daley, T., 2003, Pressure and fluid saturation prediction in a multicomponent reservoir using combined seismic and electromagnetic imaging: Geophysics, 68, 1580-1591.

McGillibray, P. R., Oldenburg, D. W., Ellis, R. G., and Habashy, T. M., 1994, Calculation of sensitivities for the frequency-domain electromagnetic problem: Geophys. J. Int., 116, 1-4.

Oldenburg, D. W., McGillivray, R. R., and Ellis, R. G., 1993, Generalized subspace methods for large-scale inverse problems: Feophys. J. Internat., 114, 12-20.

Spies, B. R., and Habashy, T. M., 1995, Sensitivity analysis of crosswell electromagnetics: Geophysics, 60, 834-845.

Tseng, H.-W., Lee, K. H., and Becker, A., 2003, 3D interpretation of electromagnetic data using a modified extended Born approximation: Geophysics, 68, 127-137.

Vesnaver, A., and Bohm, G., 2002, One, none, hundred thousands tomographic images: The Oil Drop, 14, 2-10.

Wannamaker, P. E., Hohmann, G. W., and San Filipo, W. A., 1984, Electromagnetic modeling of three-dimensional bodies in layered earths using integral equations: Geophysics, 49, 60-74.

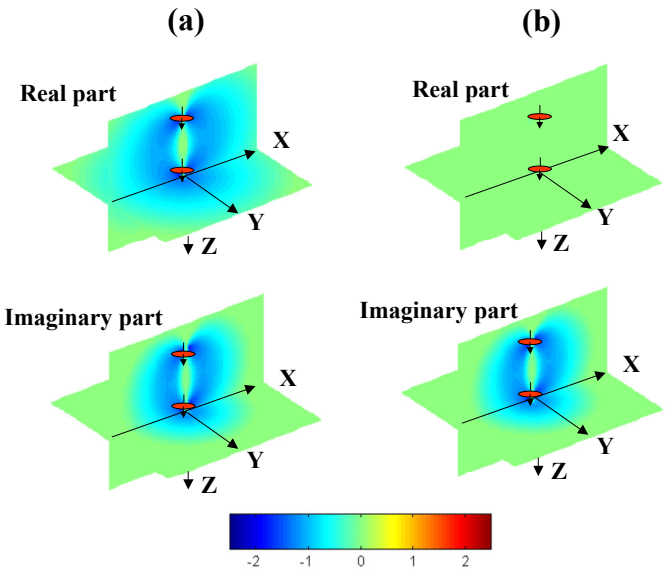

Fig. 1 Sensitivity function for a pair of co-axial transmitter-receiver configuration. (a) Logarithm of the sensitivity normalized to the maximum of the function in the whole domain. (b) Logarithm of the sensitivity normalized to the primary field calculated at the receiver.

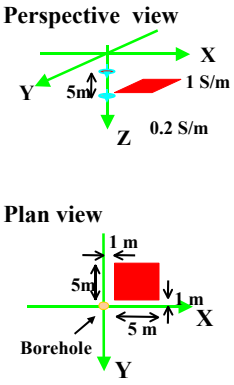

Fig. 2 A thin conductive plate model used for producing synthetic data for verifying the MEBA algorithm for single-hole EM surveys.

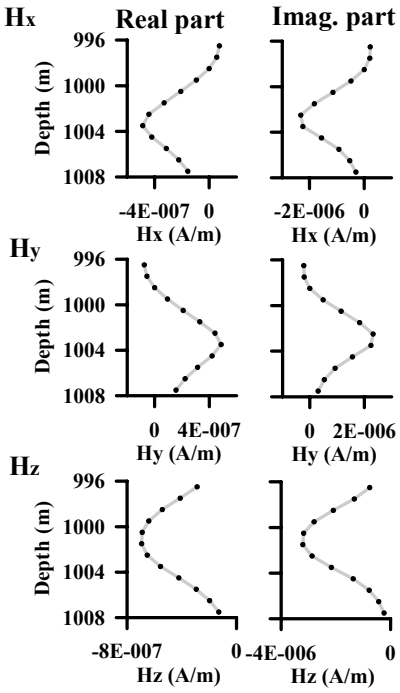

Fig. 3 Calculated magnetic fields due to a vertical magnetic source for the model presented in Figure 2.

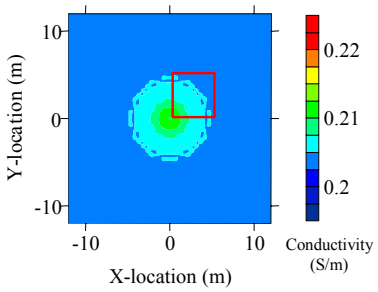

Fig. 4 Inverted conductivity on a horizontal plane at the level of the conductive plate shown in Figure 2. Only vertical magnetic field is used for inversion.

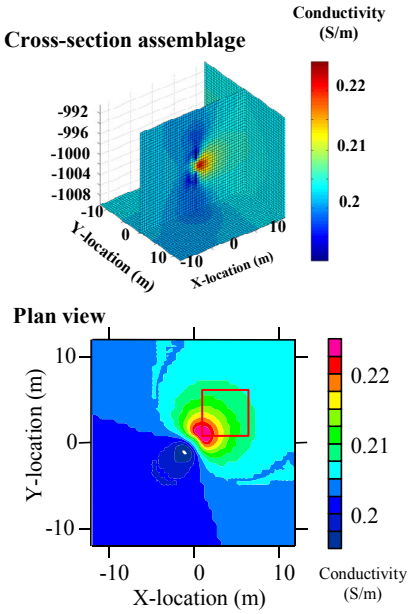

.

Fig. 5 Inverted conductivity on a horizontal plane at the level of the conductive plate shown in Figure 2. All the three component magnetic fields are used for inversion

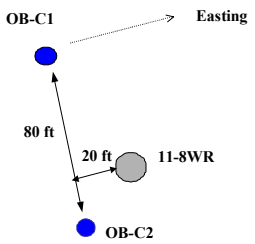

Fig. 6 Surface projection of the boreholes related to single-hole EM data collection.

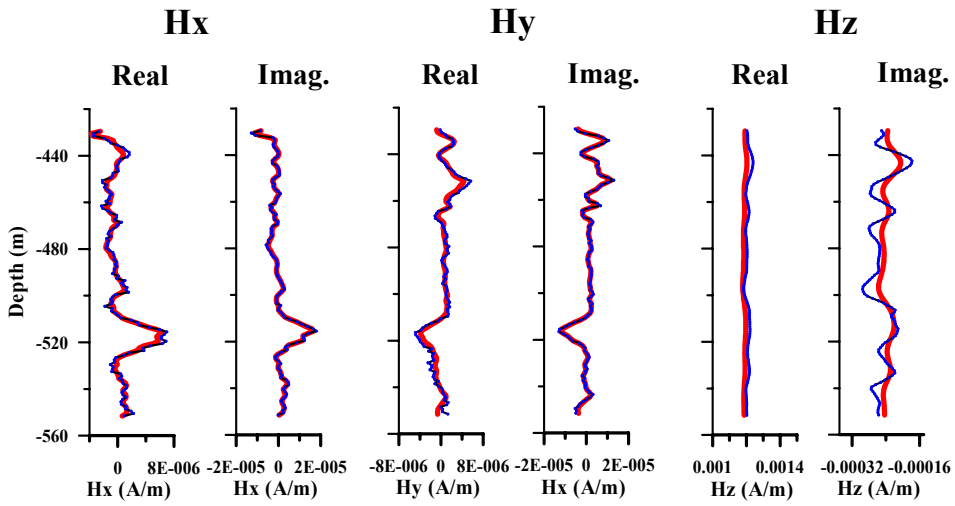

Fig. 7 Single-hole magnetic field data (in blue) in OB-C1 used for inversion. The simulation data for the inversion results are presented in red.

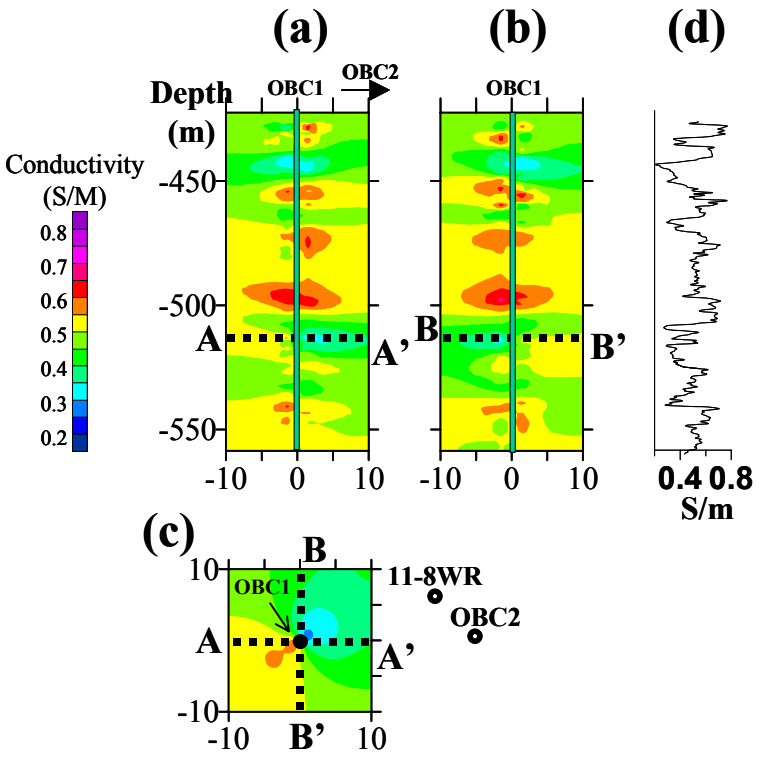

Fig. 8 Inversion results: (a) in the vertical plane containing OB-C1 and OB-C2; (b) an east-west vertical plane centered at OB-C1; (c) horizontal slice centered at OB-C1 at the depth of 513 m. Surface projection of 11-8WR, the injection well, and OBC2, another observation well, are also displayed. (d) Induction logging for OB-C1 at the start of the CO_2 injection.

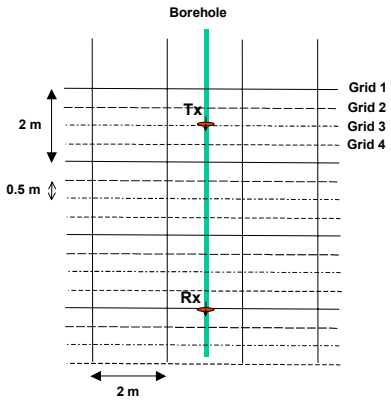

Figure 9 The four model grids relative to Transmitter location.

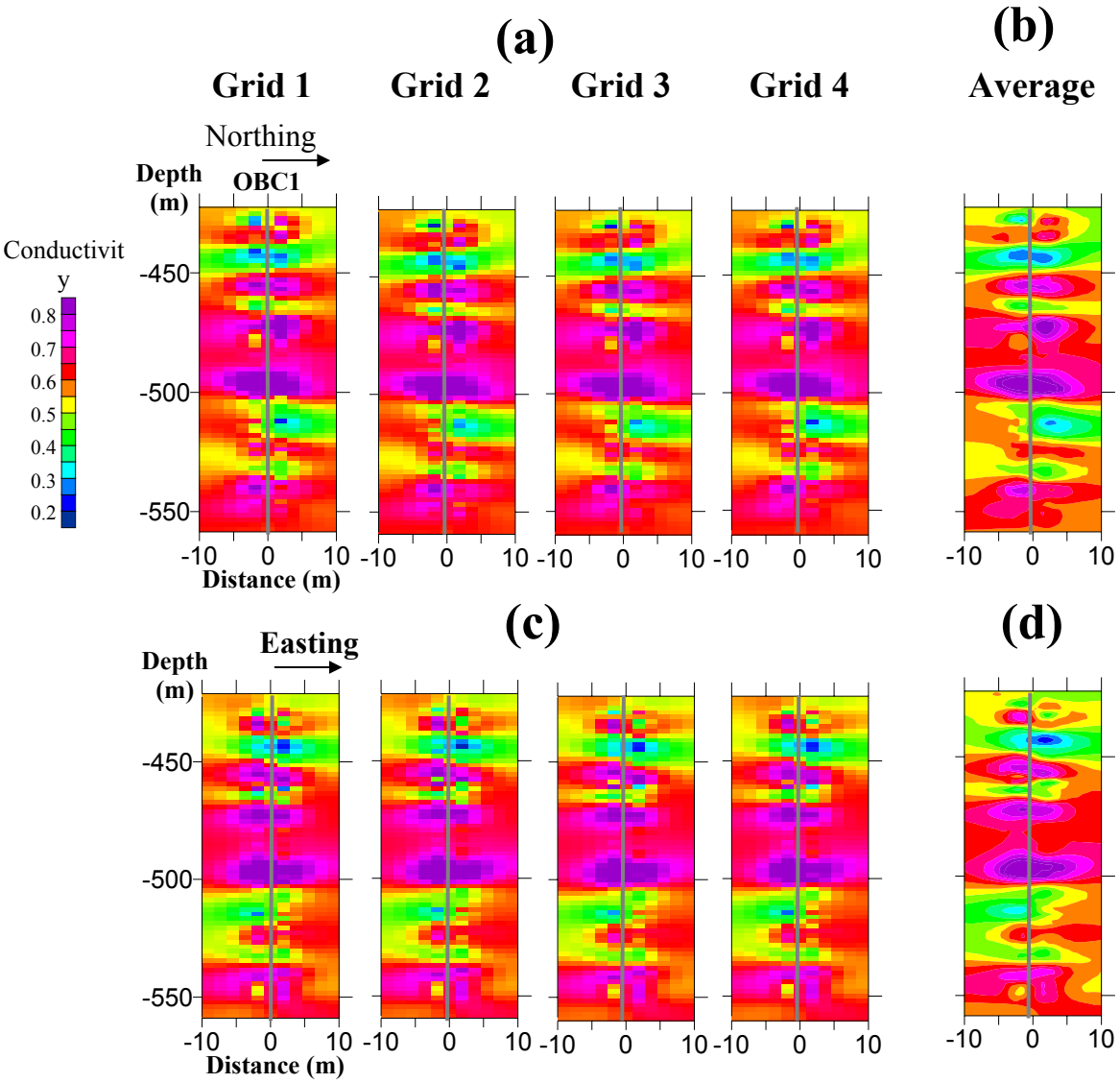

Fig. 10 Inversion results for the four griddings: (a) the vertical plane containing OB-C1 and OB-C2; (b) the averaged conductivity from (a); (c) east-west vertical plane centered at OB-C1; and (d) averaged conductivity from (c).